

Accepted Manuscript

Structural versatility driven by the flexible di(4-pyridyl) sulfide ligand: from mononuclear cobalt(II) species to sheet-like copper(II) architectures

Natalia V. Reis, Maria Vanda Marinho, Tatiana Renata G. Simões, Karina C. Metz, Raphael C. Vaz, Willian X.C. Oliveira, Cynthia L.M. Pereira, Wdeson P. Barros, Carlos B. Pinheiro, Siddhartha O.K. Giese, David L. Hughes, Kleber R. Pirota, Wallace C. Nunes, Humberto O. Stumpf

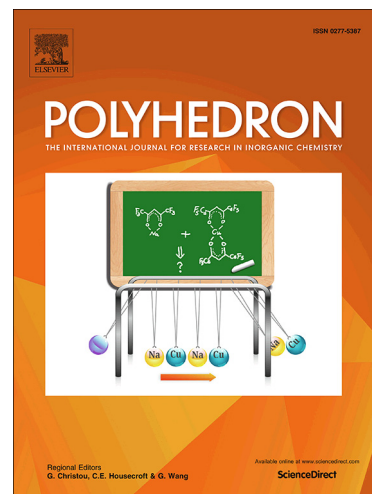
PII: S0277-5387(19)30475-9
DOI: <https://doi.org/10.1016/j.poly.2019.07.005>
Reference: POLY 14055

To appear in: *Polyhedron*

Received Date: 1 May 2019
Accepted Date: 6 July 2019

Please cite this article as: N.V. Reis, M. Vanda Marinho, T.R.G. Simões, K.C. Metz, R.C. Vaz, W.X.C. Oliveira, C.L.M. Pereira, W.P. Barros, C.B. Pinheiro, S.O.K. Giese, D.L. Hughes, K.R. Pirota, W.C. Nunes, H.O. Stumpf, Structural versatility driven by the flexible di(4-pyridyl) sulfide ligand: from mononuclear cobalt(II) species to sheet-like copper(II) architectures, *Polyhedron* (2019), doi: <https://doi.org/10.1016/j.poly.2019.07.005>

This is a PDF file of an unedited manuscript that has been accepted for publication. As a service to our customers we are providing this early version of the manuscript. The manuscript will undergo copyediting, typesetting, and review of the resulting proof before it is published in its final form. Please note that during the production process errors may be discovered which could affect the content, and all legal disclaimers that apply to the journal pertain.



**Structural versatility driven by the flexible di(4-pyridyl) sulfide ligand:
from mononuclear cobalt(II) species to sheet-like copper(II)
architectures****

Natalia V. Reis,^a Maria Vanda Marinho,^b Tatiana Renata G. Simões,^c Karina C. Metz,^c
Raphael C. Vaz,^a Willian X. C. Oliveira,^a Cynthia L. M. Pereira,^a Wdeson P. Barros,^d
Carlos B. Pinheiro,^e Siddhartha O. K. Giese,^c David L. Hughes,^f Kleber R. Pirota,^g
Wallace C. Nunes,^h and Humberto O. Stumpf.^{a,*}

^a*Departamento de Química, ICEx, Universidade Federal de Minas Gerais, Belo Horizonte, Minas Gerais, 31270-901, Brazil.*

^b*Instituto de Química, Universidade Federal de Alfenas, Alfenas, Minas Gerais, 37130-001, Brazil.*

^c*Departamento de Química, Universidade Federal do Paraná, Curitiba, Paraná, 81531-980, Brazil.*

^d*Instituto de Química, Universidade Estadual de Campinas, Campinas, São Paulo, 13083-970, Brazil*

^e*Departamento de Física, ICEx, Universidade Federal de Minas Gerais, Belo Horizonte, Minas Gerais, 31270-901, Brazil.*

^f*School of Chemistry, University of East Anglia, Norwich NR4 7TJ, UK.*

^g*Instituto de Física Gleb Wataghin, Universidade Estadual de Campinas, Departamento de Física da Matéria Condensada, Campinas, SP 13083-970, Brazil*

^h*Instituto de Física, Universidade Federal Fluminense, Av. Gal. Milton Tavares de Souza, s/nº, Campus da Praia Vermelha, 24210-346, Niterói, Rio de Janeiro, Brazil.*

**corresponding author: stumpf@ufmg.br (H.O. S.)*

** This work is dedicated to Prof. Miguel Julve from Universitat de València, Spain, in reason of his 65th birthday and for being an inspiring scientist for several generations of chemists worldwide working with Molecular Magnetism.

ACCEPTED MANUSCRIPT

ABSTRACT

The reaction between the ligand di(4-pyridyl)sulfide(dps) and two salts of divalent first row transition metals ($M = \text{Co}^{2+}$, and Cu^{2+}) resulted in three new compounds with formula: $[\text{Co}(\text{dps})_4(\text{H}_2\text{O})_2](\text{ClO}_4)_2 \cdot \text{H}_2\text{O}$ (**1**), $[\text{Cu}(\text{dps})_2(\text{dmsO})_2]_n(\text{ClO}_4)_{2n}$ (**2**) and $[\{\text{Cu}(\text{dps})_2(\text{dmsO})_2\}\{\text{Cu}(\text{dps})_2(\text{dmsO})(\text{H}_2\text{O})\}]_n(\text{ClO}_4)_{4n} \cdot 2n\text{H}_2\text{O} \cdot n(\text{dmsO})$ (**3**). Crystal structures of **1-3** were determined using single-crystal X-ray diffraction. Crystal structures of **1** consists of mononuclear complexes, in which the dps ligand acts in a monodentate mode through one of the pyridyl nitrogen atoms. Compounds **2** and **3** present the dps ligand bridging metal centers leading to bidimensional coordination polymers. Magnetic properties in the polycrystalline samples of **1-3** in the 300 to 2K temperature range were investigated. Complex **1** exhibits a field-induced slow magnetization behavior and behaves as a single-ion magnet with an effective energy barrier for the reversal of magnetization of 22.9 (1.1) K and $\tau_0 = 5.3(1.2) \times 10^{-7}$ s.

Keywords: di(4-pyridyl)sulfide; cobalt(II); copper(II); coordination polymers; single-ion magnet.

1. Introduction

The research interest on well-known ligands such as pyridyl derivatives has rapidly overgrown in the last decade [1]. Possibly it is due to their ability to form not only discrete coordination complexes able to act as Secondary Building Units (SBUs) but also in the building of coordination polymers (CPs) [1], porous coordination polymers (PCPs, also known as metal-organic frameworks or MOFs) [2-4], and spin crossover systems (SCO) [2]. The structures and properties of these systems can be controlled by choosing the appropriate bridging ligands, metal ions, counterions, as well as the solvents employed on the synthesis [5-6].

To achieve coordination compounds with different dimensionalities and molecular architectures [7], flexible ligands can be used as SBUs. In this way, dealing with ligands containing pyridine rings [1, 8-13], as well as pyridine ligands connected through sulfur atoms [4, 14], di(4-pyridyl) sulfide (dps) [1, 15-17] can be considered a synthetic strategy to be explored to obtain different systems [2].

A recent example reported in the literature that shows the flexibility of dps ligand in the $[\text{Cu}_2(\text{O}_2\text{CC}_8\text{H}_9)_4(\text{dps})]_n$ paddle-wheel complex giving waving chains [1]. The crystal structure shows the value of the copper-copper distance through the dps ligand is 10.2571(7) Å consisting of paddle-wheel dicopper(II) units interlinked by dps ligands. From a magnetic point of view, this compound could be viewed as isolated dinuclear entities of $\text{Cu}_2(\text{carboxylate})_4$. The negligible exchange magnetic coupling through the dps ligand was confirmed through magnetic measurements. Other examples also show that the extended double dps bridges are very poor mediators of magnetic interactions between the copper(II) ions [16, 18]. The magnetic behavior observed in the $[\text{Cu}_2(\text{O}_2\text{CC}_8\text{H}_9)_4(\text{dps})]_n$ system is due to the presence of interactions between copper(II) ions through carboxylate groups [1, 19].

Several examples of systems obtained using dps ligand were summarized (compounds published from 2006 to 2018) in Table S1 in the Supporting Information (SI) highlighting the choice of this ligand for this work. These systems include discrete compounds [15, 20-21], one-dimensional (1-D) [1, 14-17, 19, 22], two-dimensional (2-D) [7, 21, 23-25] and three-dimensional (3-D) [26-28] coordination polymers in addition to 3D metal-organic frameworks [24, 29-30] and sandwich-like structure [31].

Herein, we report the synthesis and structural characterization of three new compounds obtained from dps ligand formulated as: $[\text{Co}(\text{dps})_4(\text{H}_2\text{O})_2](\text{ClO}_4)_2 \cdot \text{H}_2\text{O}$ (**1**), $[\text{Cu}(\text{dps})_2(\text{dmsO})_2]_n(\text{ClO}_4)_{2n}$ (**2**) and $[\{\text{Cu}(\text{dps})_2(\text{dmsO})_2\} \{\text{Cu}(\text{dps})_2(\text{dmsO})(\text{H}_2\text{O})\}]_n(\text{ClO}_4)_{4n} \cdot 2n\text{H}_2\text{O} \cdot n(\text{dmsO})$ (**3**). **1** is a mononuclear complex while compounds **2** and **3** are bidimensional coordination polymers.

2. Experimental Section

2.1. Materials

Copper(II) perchlorate hexahydrate, cobalt(II) perchlorate hexahydrate, methanol, dimethylsulfoxide were purchased from Sigma-Aldrich and used as received. Di(4-pyridyl)sulfide (dps) ligand was prepared according to a previously reported procedure [15].

Caution! Although no problems in this work were encountered, care should be taken when manipulating such potentially explosive chemicals as perchlorate ions in the presence of organic matter.

2.2. Syntheses of the complexes

2.2.1. Synthesis of $[\text{Co}(\text{dps})_4(\text{H}_2\text{O})_2](\text{ClO}_4)_2 \cdot \text{H}_2\text{O}$ (**1**)

Compound **1** was synthesized by mixing an aqueous solution (5 ml) of $\text{Co}(\text{ClO}_4)_2 \cdot 6\text{H}_2\text{O}$ (0.110 g, 0.30 mmol for **1**) with 5 mL of a methanolic solution of dps (0.028 g, 0.15 mmol). After 15 min of stirring, the resulting solution was left to stand at room temperature (25 °C). A week later, orange needles (**1**) single-crystals suitable for X-ray diffraction analysis were collected, filtered and dried in air. Yield: 73% (**1**). Anal. calcd for $\text{C}_{40}\text{H}_{38}\text{Cl}_2\text{CoN}_8\text{O}_{11}\text{S}_4$ (%): C, 45.1; H, 3.6; N, 10.5; Co, 5.5 %. Found: C, 45.0; H, 3.3; N, 10.4 and Co, 5.6 %. IR (KBr, cm^{-1}) for **1**: 1578, 1540, 1482, 1412 ($\nu_{\text{CC/CN}}\text{dps}$); 1112, 1100, 1088, 1060 ($\nu_{\text{Cl-O}}\text{ClO}_4$); 814, 828 ($\nu_{\text{CS}}\text{dps}$); 708, 720 (δ_{CH}); 624 ($\delta_{\text{O-Cl-O}}$).

2.2.2. Synthesis of $\{[\text{Cu}(\text{dps})_2(\text{dmsO})_2](\text{ClO}_4)_2\}_n$ (**2**)

To a solution of $\text{Cu}(\text{ClO}_4)_2 \cdot 6\text{H}_2\text{O}$ (0.019 g, 0.05 mmol) in 5 mL H_2O , a solution of dps (0.009 g, 0.05 mmol) in 5 mL of CH_3OH was added. Thereafter, 1 ml of dmsO was added and the blue resulting solution was maintained under stirring for ten minutes at room temperature. The solution was allowed to evaporate at room temperature and after a week blue prismatic single-crystals, suitable for X-ray diffraction, were collected. Yield: 66%. Anal. calcd. for $\text{C}_{24}\text{H}_{26}\text{Cl}_2\text{CuN}_4\text{O}_{10}\text{S}_4$ (%): C, 36.3; H, 3.6; N, 7.1 and Cu, 8.0 %. Found: C, 35.9; H, 3.1; N, 7.1 and Cu, 8.2%. IR (KBr, cm^{-1}): 1593, 1537, 1485, 1420 ($\nu_{\text{CC/CN}}\text{dps}$); 1107, 1091, 1059, 1023 ($\nu_{\text{Cl-O}}\text{ClO}_4$); 824, 729 (ν_{CS}); 624 ($\delta_{\text{O-Cl-O}}$)

2.2.3. Synthesis of $[\{[\text{Cu}(\text{dps})_2(\text{dmsO})_2]\{[\text{Cu}(\text{dps})_2(\text{dmsO})(\text{H}_2\text{O})]\}_n](\text{ClO}_4)_{4n} \cdot 2n(\text{H}_2\text{O}) \cdot n(\text{dmsO})$ (**3**)

A mixture of dmsO and water (1:3v/v) was added carefully layered onto a 5.0 mL dmsO solution containing $\text{Cu}(\text{ClO}_4)_2 \cdot 6\text{H}_2\text{O}$ (37 mg, 0.10 mmol) and dps (19 mg, 0.10 mmol). Then a water layer (2 mL) was added on the top. After a week, green crystals suitable for X-ray diffraction were grown and collected by filtration. Yield: 41%. Anal. calcd. for $\text{C}_{48}\text{H}_{60}\text{Cl}_4\text{Cu}_2\text{N}_8\text{O}_{22}\text{S}_8$ (%): C, 35.5; H, 3.7; N, 6.9 and Cu, 7.8 %. Found: C, 35.4; H, 3.3;

N, 6.8 and Cu, 7.2 %. IR (KBr, cm^{-1}): 1592, 1536, 1484, ($\nu_{\text{CC/CN}}\text{dps}$); 1110, 1091, 1060, ($\nu_{\text{Cl-OClO}_4}$); 824, 729 (ν_{CS}); 626 ($\delta_{\text{O-Cl-O}}$).

2.3. Physical Measurements

Elemental analyses (C, H, N) were performed with a PerkinElmer 2400 analyzer. The IR spectrum of **1-3** was recorded on a Bomem Michelson 102 FTIR spectrophotometer using KBr pellets in the range $4000\text{--}400\text{ cm}^{-1}$ with an average of 128 scans and 4 cm^{-1} of spectral resolution. The samples **1-3** were verified by powder X-ray diffraction (PXRD) measurements performed on a Rigaku / Geirgflex (for **1-2**) in the aluminum sample holder and on a Shimadzu XRD – 6000 (for **3**) with a scan speed of $4^\circ/\text{min}$ setup in $\theta\text{-}2\theta$ geometry using Cu $K\alpha$ radiation. Magnetic susceptibility measurements of crushed polycrystalline samples of **1-3** were carried out on a Quantum Design MPMS-XL7 SQUID magnetometer and on a Cryogenic S700 SQUID magnetometer in the temperature range of 2-300 K, under an applied dc field of 0.1 T (for DC measurements) and a Quantum Design PPMS (for AC susceptibility measurements). Diamagnetic corrections were applied to the observed paramagnetic susceptibilities using Pascal's constants [32-33]: -551.24×10^{-6} for **1**, -391.48×10^{-6} for **2** and -405.48×10^{-6} for **3** (per mol of cobalt(II) or copper (II) ions). Experimental susceptibilities were also corrected for the temperature-independent paramagnetism [$60 \times 10^{-6}\text{ cm}^3\text{ mol}^{-1}$ per mol of copper(II) ions] and the sample holder.

2.4. X-ray data collection and refinements

The single-crystal X-ray data were collected on an Oxford-Diffraction Gemini-Ultra diffractometer (**1** and **2**) and Bruker D8 Venture diffractometer equipped with a Photon-100 CMOS detector and a Kryoflex II cooling device (**3**). Experiments were performed

with a graphite monochromatic radiation source (Mo-K α , $\lambda = 0.71073 \text{ \AA}$ or Cu-K α $\lambda = 1.5418 \text{ \AA}$), under low-temperature nitrogen flux (See Table 1). Suitable crystals were mounted in the noncrystalline polyamide sample holder (MicroMountTM 100 μM (MiTeGen). Reduction of the data and analytical absorption corrections were performed using the CrysAlis [34] (**1** and **2**) and APEX3 [35] (**3**) suites. Space group identification was done with XPREP [36], and structure solution was carried out by direct methods using Superflip [37-38] (**1** and **2**) and intrinsic phasing methods in SHELXT [39-40] (**3**). All structures were refined by full-matrix least-squares methods against F^2 in the program SHELXL [41]. All atoms (except hydrogen atoms) were refined with anisotropic atomic displacement parameters. All hydrogen atoms, except for H40A, H40B, H50A, and H50B in structure (**3**), were located in difference maps and included as fixed contributions according to the riding model [42]. For organic moieties C–H = 0.97 \AA and $U_{\text{iso}}(\text{H}) = 1.5 U_{\text{eq}}(\text{C})$ for methyl groups (C/N)–H = 0.97 \AA and $U_{\text{iso}}(\text{H}) = 1.2 U_{\text{eq}}(\text{C/N})$ for aromatic carbon and amide nitrogen atoms and finally O–H = 0.90 \AA and $U_{\text{iso}}(\text{H}) = 1.5 U_{\text{eq}}(\text{O})$ for water molecules. Absorption corrections were carried out using analytical numeric methods using a multifaceted crystal model [43]. All structures are chiral, and the correct configuration was determined by the Flack parameter based on the Parsons method of quotients[44] (See Table 1). Molecular graphics were produced with the ORTEP[45] and MERCURY[46] programs. CCDC 1880908 (**1**), 1880910 (**2**), and 1880911 (**3**) contain the supplementary crystallographic data for this paper. These data can be obtained free of charge from the Cambridge Crystallographic Data Centre. Crystal data and details of the data collection and refinement for **1-3** are listed in Table 1 and selected bond distances and angles are given in Table 2.

3. Results and Discussion

3.1. General Characterization

The IR spectra of all complexes were performed by KBr pellets in the range of 4000-400 cm^{-1} . The spectra of the compounds **1-3** show a characteristic absorption band at $\sim 1580 \text{ cm}^{-1}$ attributed to CC and CN stretching vibrations of the pyridyl ring from dps ligand. The spectra also show typical absorption bands of ClO_4^- counteranions with strong bands in the range 1112-1060 cm^{-1} and at $\sim 622 \text{ cm}^{-1}$ assigned to stretching vibrations of ClO_4^- groups [21, 47-48]. The IR spectra of **2** and **3** are very similar, with the presence of a peak at 1023 cm^{-1} which is attributed to stretching vibration of the S-O bond of the dmsO molecule of crystallization [49]. The broad band centered at *ca.* 3400 cm^{-1} indicate the O-H stretching vibration of water molecules for complexes **1**.

The X-ray powder diffraction patterns of **1-3** (Supporting Information, Figures S1-S3) match the simulated ones from their respective crystallographic structures.

3.2. Description of the Structures

3.2.1. Crystalline Structures of **1-3**

The structure of **1** was determined by single-crystal X-ray diffraction analysis. It crystallizes in the chiral tetragonal system and space group $P4_12_12$. The $\text{Co}(\text{dps})_4$ mononuclear entity **1** is intrinsically chiral due to its propeller-like shape, which results from the tilt of each bound pyridine ring with respect to the metal basal plane. This structural feature would lead to different enantiomers that could explain the crystallization in a chiral tetragonal system for **1**. The structure of **1** consists of discrete cobalt(II) complexes, with the metal ion linked to four dps ligands and two water molecules, with a further molecule of water of crystallization and two perchlorate anions to achieve neutrality. Figure 1 shows the crystal structure of **1**, where the Co^{2+}

coordination sphere exhibits a distorted octahedral geometry. The metal ion is surrounded by four nitrogen atoms [N1, N3, N1ⁱ, N3ⁱ; symmetry code (i) = $y, x, -z$] from four dps ligands in the basal plane acting in a monodentate fashion. Two oxygen atoms [O1, O1ⁱ] from two water molecules are found capping the octahedron leading the cobalt atom in a *trans*-N₄O₂ coordination sphere. The equatorial Co–N bond distances vary from 2.180(5) to 2.142(5) Å, and the axial Co–O1 distance is 2.098(4) Å indicating a compression along O1–Co1–O1ⁱ direction, the main cause of the octahedron distortion in this compound.

The supramolecular structure is mainly a result of the hydrogen bonds (Table S2). The interaction net involves the coordinated water molecule, the crystallization water molecule, and both free pyridyl groups of dps. The free crystallization water molecule acts binding two *cis* dps ligands [O6⋯N4 = 2.866(9) Å]. To this water molecule is found two coordinated water molecules as hydrogen donors [O1⋯O6ⁱⁱ = 2.777(6) Å, symmetry code (ii) = $-y+3/2, x-1/2, z-1/4$]; O1 is also hydrogen donor to the free pyridyl groups [O1⋯N2ⁱⁱⁱ = 2.810(4) Å, symmetry code (iii) = $-x+3/2, y+1/2, -z+1/4$]. Although the perchlorate anion presents electron donor oxygen atoms, in this compound no hydrogen bonds were found involving this group, having no other function than filling free space and grant the neutrality of the resulting solid. This anion is located in cages formed by dps pyridyl groups. In this crystal packing the metallic ions are very far from each other, being the closest ones at 8.300(4) Å [Co1⋯Co1^{iv}; symmetry code (iv) = $1-x, 1-y, 1/2+z$].

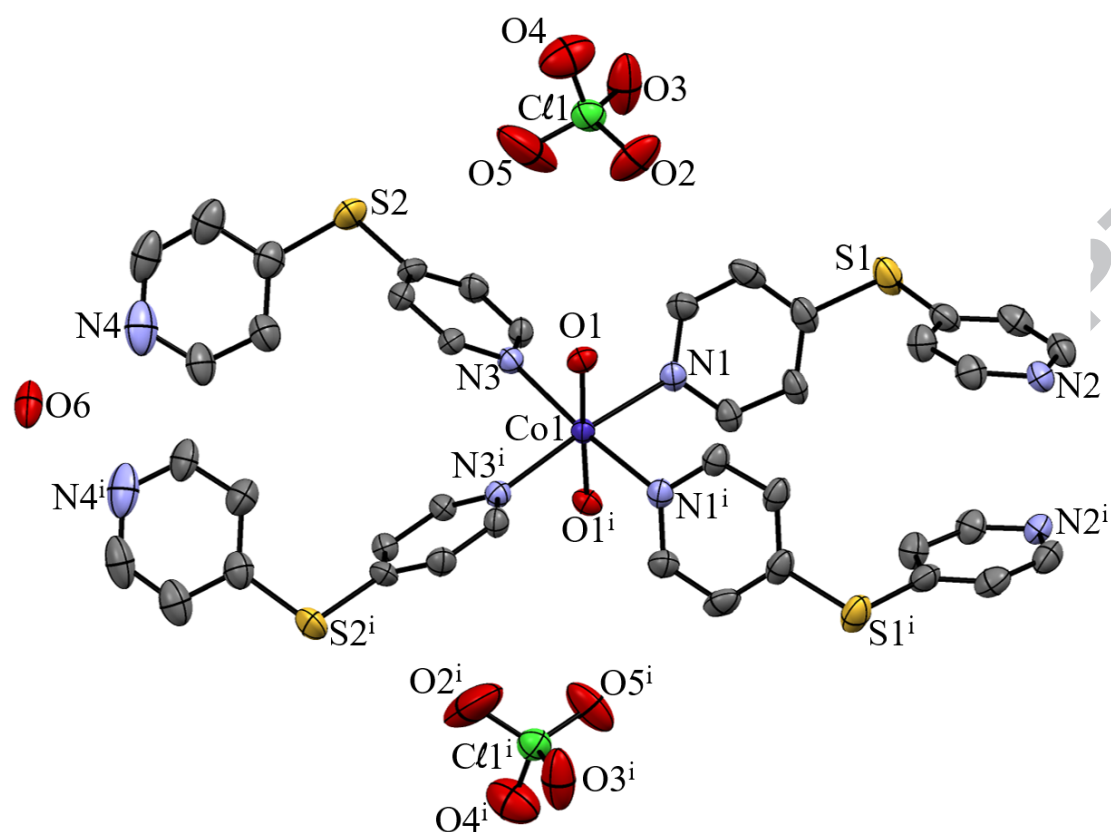


Figure 1: View of the crystal structure depicting the metal surroundings in compound **1** with the numbering of the non-hydrogen and non-carbon. Thermal ellipsoids are drawn at the 50% probability level, and the hydrogen atoms are omitted for clarity. Symmetry code: (i) $x, y, -z$.

Table 1. Summary of the Crystal Data and Refinement Details for **1-3**.

| Compound | 1 | 2 | 3 |
|--|----------------------------------|----------------------------------|------------------------------------|
| <i>Formula</i> | $C_{40}H_{38}N_8O_{11}S_4Cl_2Co$ | $C_{24}H_{28}N_4O_{10}S_4Cl_2Cu$ | $C_{48}H_{60}N_8O_{22}S_8Cl_4Cu_2$ |
| <i>F_w /g mol⁻¹</i> | 1064.85 | 795.18 | 1626.40 |
| <i>T /K</i> | 150(2) | 150(2) | 100(2) |
| <i>λ /Å</i> | 1.5418 | 0.71073 | 0.71073 |
| <i>Crystal System</i> | Tetragonal | Orthorhombic | Monoclinic |

| | | | |
|---|--------------------|--------------------|-------------------|
| <i>Space group</i> | $P4_12_12$ | $Pna2_1$ | Pc |
| $a / \text{\AA}$ | 16.56460(10) | 17.2950(2) | 17.0067(8) |
| $b / \text{\AA}$ | 16.56460(10) | 10.99370(10) | 10.9400(5) |
| $c / \text{\AA}$ | 16.59390(10) | 17.2035(3) | 17.8529(9) |
| $\alpha / ^\circ$ | 90 | 90 | 90 |
| $\beta / ^\circ$ | 90 | 90 | 90.143(3) |
| $\gamma / ^\circ$ | 90 | 90 | 90 |
| $V / \text{\AA}^3$ | 4553.13(6) | 3271.01(7) | 3321.6(3) |
| Z' | 4 | 4 | 2 |
| $\rho / \text{Mg m}^{-3}$ | 1.553 | 1.615 | 1.626 |
| μ / mm^{-1} | 6.335 | 1.145 | 1.131 |
| $F(000)$ | 2188 | 1628 | 1668 |
| <i>Crystal size/ mm³</i> | 0.16 x 0.16 x 0.88 | 0.10 x 0.32 x 0.58 | 0.11x 0.19 x 0.26 |
| <i>Reflections collected (Rint)</i> | 67024 (0.029) | 100794 (0.020) | 127071 (0.093) |
| <i>Unique Reflections / Parameters / Restraints</i> | 4011 / 308 / 7 | 6698 / 407 / 1 | 15239 / 850 / 4 |
| <i>Reflections with $I > 2\sigma(I)$</i> | 3754 | 6258 | 12341 |
| <i>Goodness-of-fit on F^2</i> | 1.024 | 1.056 | 1.030 |
| R_a, wR_b (all data) | 0.0550, 0.1426 | 0.0395, 0.0988 | 0.063, 0.078 |
| <i>Flack Parameter, Quotients used</i> | -0.016(4), 1465 | 0.050(6), 2896 | 0.004(5), 5214 |
| <i>Larg. diff. peak and hole / e \AA^{-3}</i> | 1.244, -0.338 | 1.831, -0.469 | 0.704, -0.482 |

ACCEPTED MANUSCRIPT

Table 2 – Main metal-ligand bond lengths and angles

| 1 ^e | | 2 [#] | | 3 [£] | | | | | | | |
|------------------|-----------------|--------------------------------------|-----------------|----------------------|-----------------|---------------------------------------|-------------|----------------------|-----------|---------------------------------------|-------------|
| M–L distance / Å | L–M–L angle / ° | M–L distance / Å | L–M–L angle / ° | M–L distance / Å | L–M–L angle / ° | | | | | | |
| Co1—O1 | 2.098 (4) | O1—Co1—O1 ⁱ | 178.3 (2) | Cu1—O1 | 2.435 (4) | O1—Cu1—O2 | 176.81 (15) | Cu1—O1 | 2.374 (3) | O1—Cu1—O2 | 178.83 (13) |
| Co1—N1 | 2.179 (5) | O1—Co1—N1 | 90.56 (18) | Cu1—O2 | 2.292 (4) | O1—Cu1—N1 ⁱ | 86.06 (16) | Cu1—O2 | 2.350 (3) | O1—Cu1—N1 | 90.55 (14) |
| Co1—N3 | 2.140 (5) | O1—Co1—N1 ⁱ | 88.19 (18) | Cu1—N1 ⁱ | 2.031 (4) | O1—Cu1—N2 | 91.73 (16) | Cu1—N1 | 2.031 (4) | O1—Cu1—N2 ⁱ | 91.72 (14) |
| | | O1—Co1—N1 | 90.56 (18) | Cu1—N2 | 2.032 (4) | O1—Cu1—N3 ⁱⁱ | 92.59 (16) | Cu1—N2 ⁱ | 2.014 (4) | O1—Cu1—N3 | 88.44 (14) |
| | | O1—Co1—N3 | 86.35 (16) | Cu1—N3 ⁱⁱ | 2.027 (4) | O1—Cu1—N4 | 89.28 (16) | Cu1—N3 | 2.020 (4) | O1—Cu1—N4 ⁱⁱ | 90.75 (14) |
| | | O1—Co1—N3 ⁱ | 94.86 (16) | Cu1—N4 | 2.032 (4) | O2—Cu1—N1 ⁱ | 91.57 (16) | Cu1—N4 ⁱⁱ | 2.040 (4) | O2—Cu1—N1 | 89.67 (14) |
| | | O1 ⁱ —Co1—N1 | 88.18 (18) | | | O2—Cu1—N2 | 90.42 (17) | Cu2—O3 | 2.319 (3) | O2—Cu1—N2 ⁱ | 89.44 (14) |
| | | O1 ⁱ —Co1—N1 ⁱ | 90.56 (18) | | | O2—Cu1—N3 ⁱⁱ | 89.77 (17) | Cu2—O4 | 2.336 (4) | O2—Cu1—N3 | 90.40 (14) |
| | | O1 ⁱ —Co1—N3 | 94.85 (16) | | | O2—Cu1—N4 | 88.63 (17) | Cu2—N5 | 2.028 (4) | O2—Cu1—N4 ⁱⁱ | 89.08 (14) |
| | | O1 ⁱ —Co1—N3 ⁱ | 86.35 (16) | | | N1 ⁱ —Cu1—N2 | 90.75 (18) | Cu2—N6 ^v | 2.051 (4) | N1—Cu1—N2 ⁱ | 88.46 (16) |
| | | N1—Co1—N1 ⁱ | 86.1 (3) | | | N1 ⁱ —Cu1—N3 ⁱⁱ | 178.63 (18) | Cu2—N7 | 2.038 (4) | N1—Cu1—N3 | 90.34 (16) |
| | | N1—Co1—N3 | 91.64 (17) | | | N1 ⁱ —Cu1—N4 | 90.91 (18) | Cu2—N8 ^{iv} | 2.034 (4) | N1—Cu1—N4 ⁱⁱ | 177.46 (17) |
| | | N1—Co1—N3 ⁱ | 174.06 (19) | | | N2—Cu1—N4 | 89.51 (17) | | | N2 ⁱ —Cu1—N3 | 178.79 (17) |
| | | N3—Co1—N3 ⁱ | 91.2 (3) | | | N2—Cu1—N4 | 178.12 (19) | | | N2 ⁱ —Cu1—N4 ⁱⁱ | 89.32 (16) |
| | | | | | | N3 ⁱⁱ —Cu1—N4 | 88.86 (18) | | | N3—Cu1—N4 ⁱⁱ | 91.88 (16) |
| | | | | | | | | | | O3—Cu2—O4 | 177.92 (14) |
| | | | | | | | | | | O3—Cu2—N5 | 90.46 (15) |
| | | | | | | | | | | O3—Cu2—N6 ^v | 87.60 (15) |
| | | | | | | | | | | O3—Cu2—N7 | 88.41 (14) |
| | | | | | | | | | | O3—Cu2—N8 ^{iv} | 94.13 (15) |
| | | | | | | | | | | O4—Cu2—N5 | 89.14 (16) |
| | | | | | | | | | | O4—Cu2—N6 ^v | 90.35 (15) |
| | | | | | | | | | | O4—Cu2—N7 | 91.95 (15) |
| | | | | | | | | | | O4—Cu2—N8 ^{iv} | 87.92 (15) |
| | | | | | | | | | | N5—Cu2—N6 ^v | 89.47 (16) |
| | | | | | | | | | | N5—Cu2—N7 | 178.54 (17) |

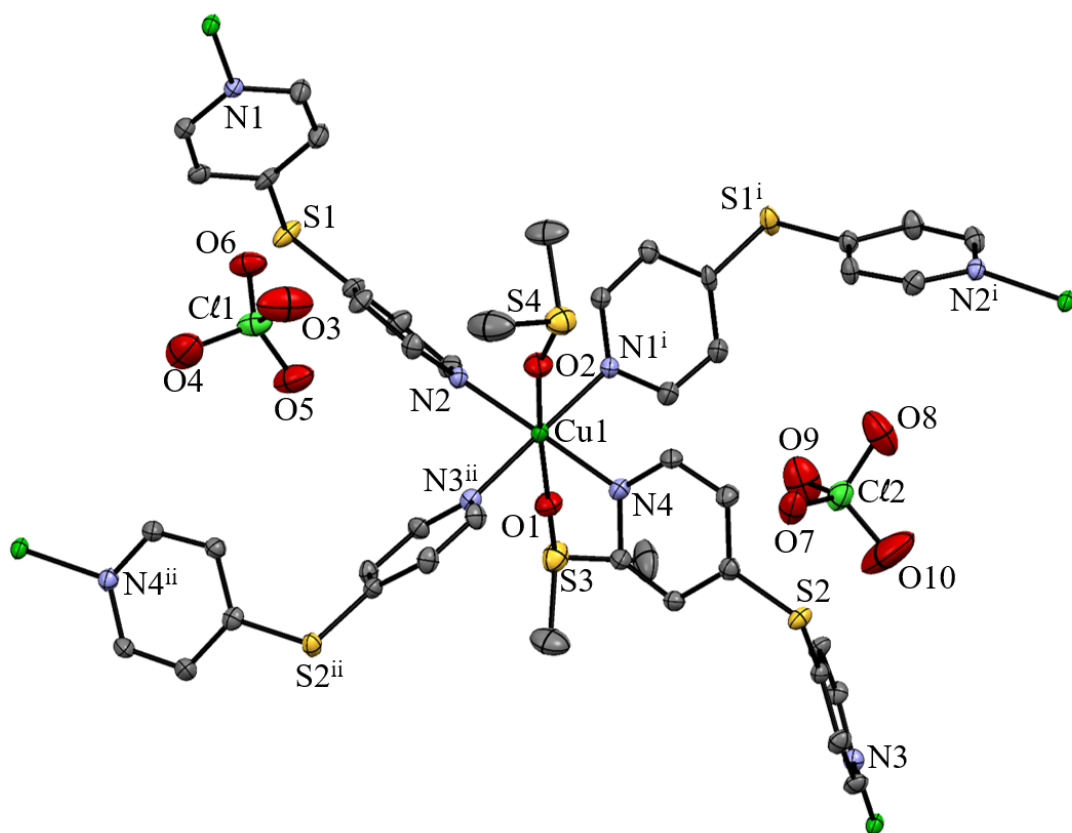
| | |
|---------------------------------------|-------------|
| N5—Cu2—N8 ^{iv} | 90.80 (16) |
| N6 ^v —Cu2—N7 | 89.57 (16) |
| N6 ^v —Cu2—N8 ^{iv} | 178.24 (17) |
| N7—Cu2—N8 ^{iv} | 90.20 (16) |

^eSymmetry code for **1**: (i) $y, x, -z$.[#]Symmetry codes for **2**: (i) $x-1/2, -y+5/2, z$; (ii) $x+1/2, -y+3/2, z$.[‡]Symmetry codes for **3**: (i) $x, -y+2, z+1/2$; (ii) $x, -y+1, z+1/2$; (iii) $x, -y+2, z-1/2$; (iv) $x, -y+1, z-1/2$; (v) $x, -y, z+1/2$; (vi) $x, -y, z-1/2$.

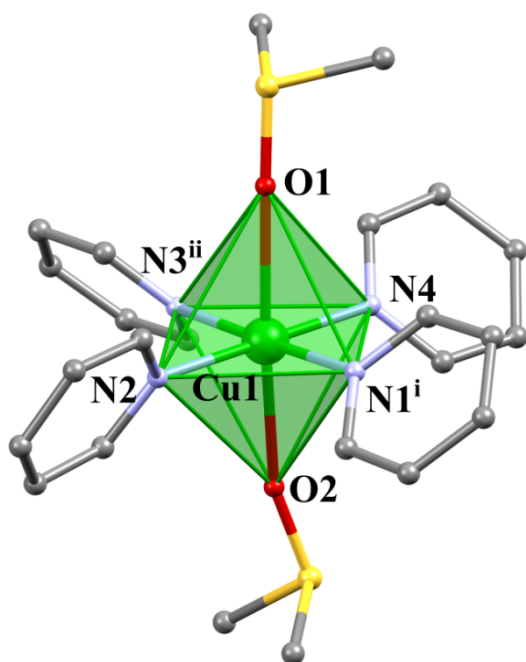
The crystal structure of **2** consists of a cationic two-dimensional network (Figure 2a) built up from *trans*-[Cu(dps)₂(dmsO)₂]²⁺ units and perchlorate anions occupying the interlayer vacancies in orthorhombic space group *Pna*2₁. Each copper(II) ion is six-coordinated in a distorted octahedral geometry; it is surrounded by four nitrogen atoms [N1, N2, N3, and N4] from four distinct dps ligands and two oxygen atoms [O1 and O2] from two dmsO molecules occupying the axial positions (Figure 2b). Furthermore, each dps acts as bidentate ligand connected to another *trans*-[Cu(dmsO)₂]²⁺ fragment, extending the network motif into polymeric sheets. The equatorial four Cu–N bonds distances are very regular varying from 2.027(4) Å to 2.032(4) Å; meanwhile the axial Cu–O distances are very different from each other, in a clear Jahn-Teller effect in this coordination axis: 2.292(4) Å [Cu1–O2] and 2.435(4) Å [Cu1–O1]. The coordination angles are all very similar, in the range of 86.1(2)° [O1–Cu1–N1] and 92.6(2)° [O1–Cu1–N3]. In each polymeric sheet, the copper(II) atoms are separated by one dps ligand, resulting in a mean separation of 10.275 Å [10.340(1) for Cu1⋯Cu1ⁱ and 10.155(1) for Cu1⋯Cu1ⁱⁱ; symmetry codes (i) = 1/2+x, 5/2–y, z; (ii) = –1/2+x, 3/2–y, z].

The crystal packing of **2** can be described as an extended parallel array of cationic layers with ClO₄[–] anions inside the cavities. These cationic layers are in direct contact, interacting by van der Waals weak forces, mainly through the dps ligands. Even with the compact layers, the metal atoms from adjacent layers are slightly farther apart than within the same layer; thus the shortest intermetallic distance is 10.481(3) Å [Cu1–Cu1^{iv}; symmetry code (iv) = –x, 2–y, –1/2+z].

(a)



(b)



(c)

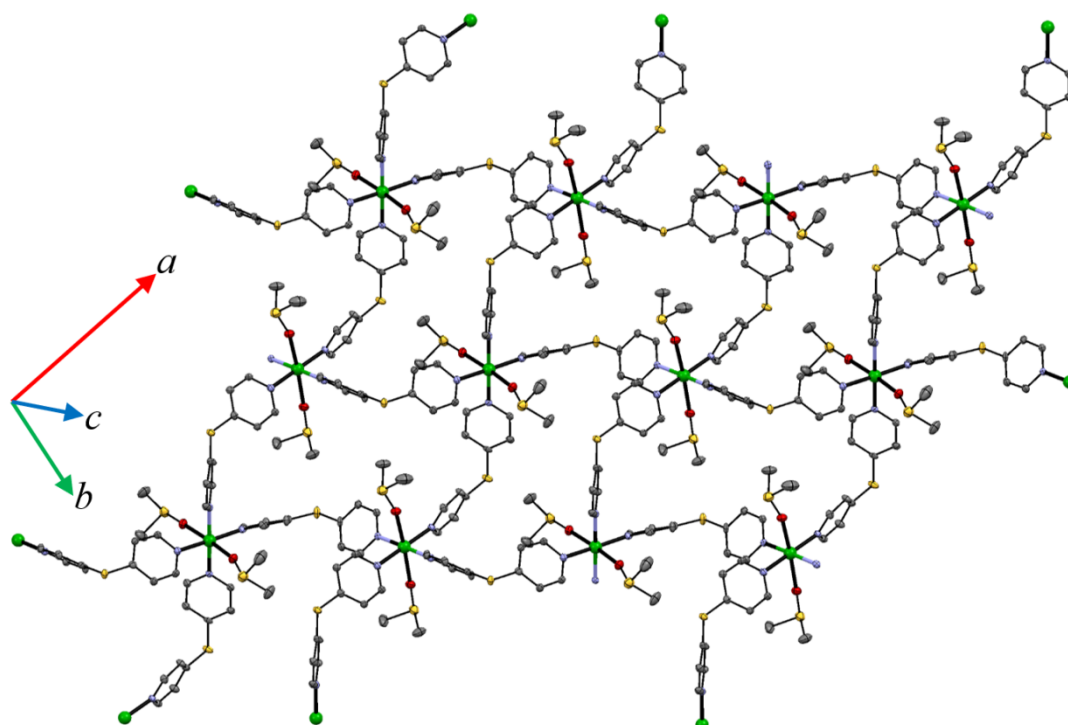


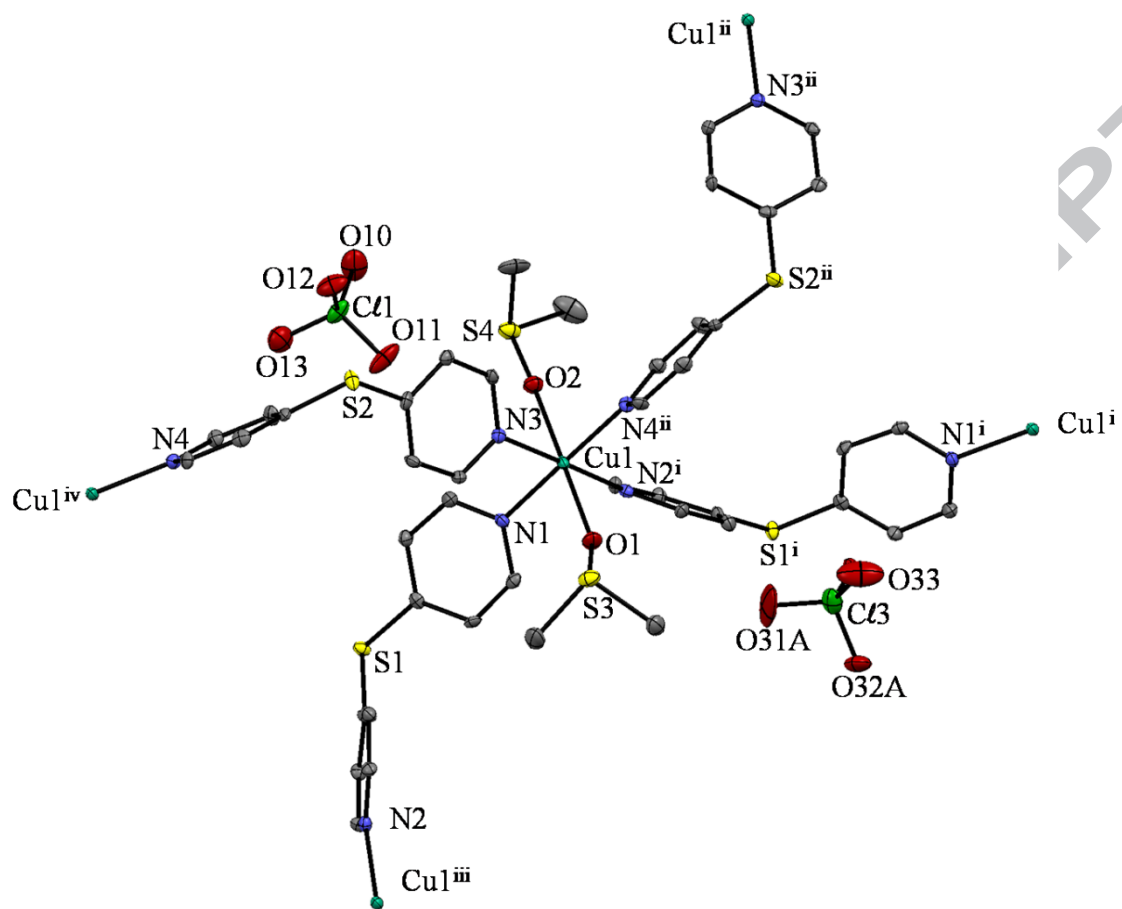
Figure 2. (a) View of the crystal structure depicting the metal surroundings in compound **2** with the numbering of the non-hydrogen and non-carbon atoms. Thermal ellipsoids are drawn at the 50% probability level, and the hydrogen atoms are omitted for clarity. (b) Copper(II) ion surroundings, showing the distorted octahedral geometry along the O–Cu–O axis. (c) View of a fragment of a cationic layer $[\text{Cu}(\text{dps})_2(\text{dmsol})_2]_n^{2n+}$ of **2** extending in the crystallographic plane ab evidencing the porous plane. Perchlorate anions were omitted for the sake of clarity. Symmetry code: (i) $x-1/2, -y+5/2, z$; (ii) $x+1/2, -y+3/2, z$; (iii) $x+1/2, -y+3/2, z$; (iv) $x-1/2, -y+5/2, z$.

The structure of **3** is also a 2D cationic coordination polymer, quite similar to **2**, containing perchlorate anions to guarantee the neutrality, but containing two non-equivalent metal ions [Cu1 and Cu2] and one water and one dmsol crystallization molecule. The Cu1 ion is six-coordinated in a distorted octahedral geometry,

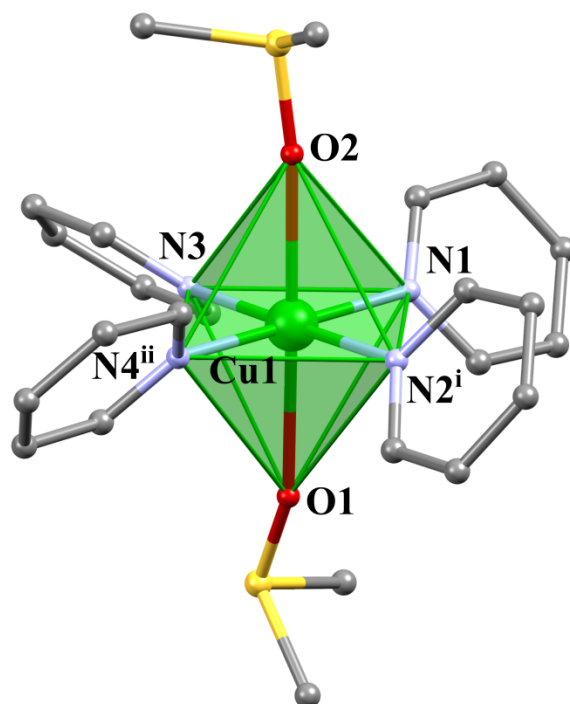
surrounded by four nitrogen atoms [N1, N2ⁱ, N3, and N4ⁱⁱ] from four dps ligands in the basal plane, and two oxygen atoms [O1 and O2] from two dmsol molecules occupying the axial positions (Figure 3a and 3b). A second copper ion, Cu2, also has a distorted octahedral geometry coordinated to four nitrogen atoms [N5, N6^v, N7 and N8^{iv}] from four dps ligands in the basal plane, and two oxygen atoms on the axial positions: O3 from the dmsol molecule and O4 from the water molecule (Figure 3c and 3d). The dps ligands connect the metal centers generating a bridged two-dimensional network, in which metal ion [Cu1] grows in a different polymer structure from that of [Cu2] (Figure 4a, 4b and S4 in SI). The three-dimensional structure consists of an extended parallel array of these two cationic layers exhibiting the ABA trend (Figure 4c) with perchlorates as counterions. The equatorial Cu–N bond distances vary from 2.014(4) to 2.040(4) Å for Cu1 and 2.028(4) to 2.051(4) Å for Cu2, while the capping Cu–O distance varies between 2.350(3)–2.374(3) Å for Cu1 and 2.319(3)–2.336(4) for Cu2. The angles about Cu1 vary from 88.44(14)° to 91.88(16)° reinforcing the distorted octahedral coordination environment of Cu²⁺ center, the angles about Cu2 are similar [87.60(15)° to 91.95(15)°]. The water molecule coordinated to Cu2 is linked to one dmsol and one water solvent molecule by hydrogen bonds, with H...O distances of 2.13 (O4–H40A...O50) and 1.88 Å (O4–H40B...O80), while another water molecule holds two perchlorate ions with hydrogen bond distances of 1.97 (O50–H50A...O41) and 1.88 Å (O50–H50B...O22) (see Table S3).

The net topologies of **2** and **3** is (4,4) rhomb layers. Their two-dimensional structures are made of rhombus-shaped Cu₄ cyclic motifs with four-connected Cu nodes and bis(monodentate) dps linkers, as depicted schematically in Figure 4.

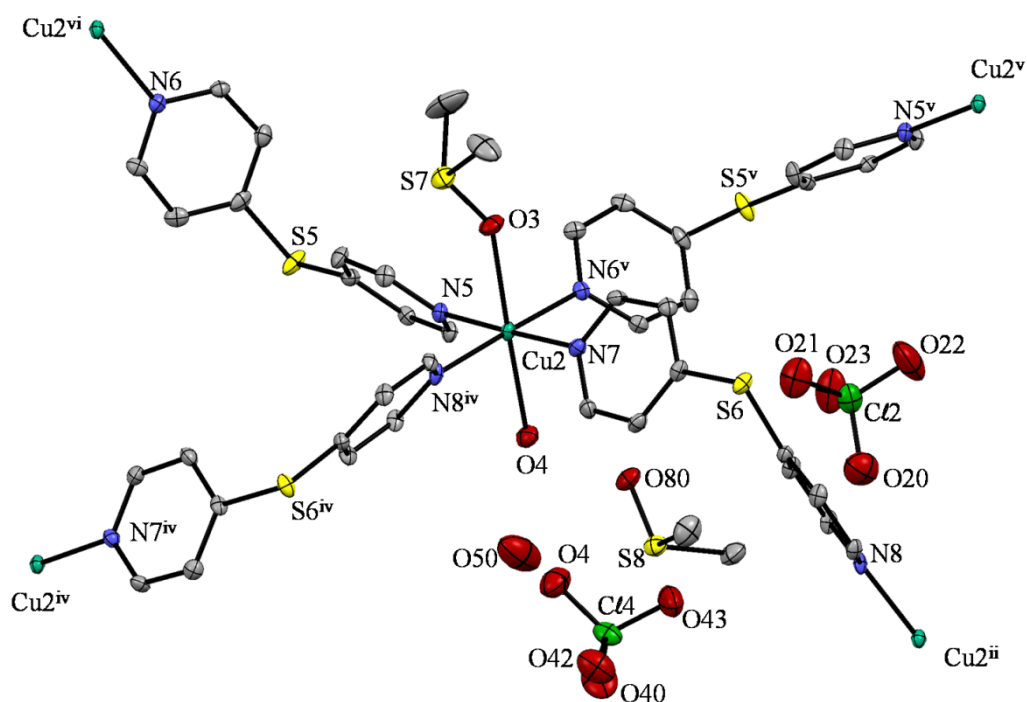
(a)



(b)



(c)



(d)

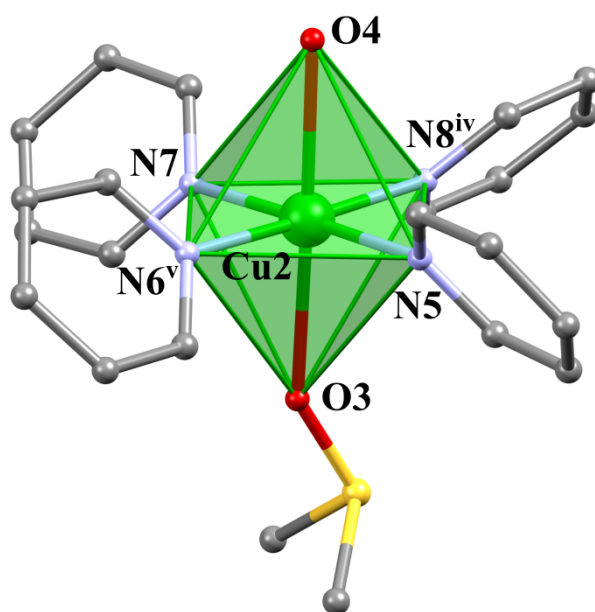
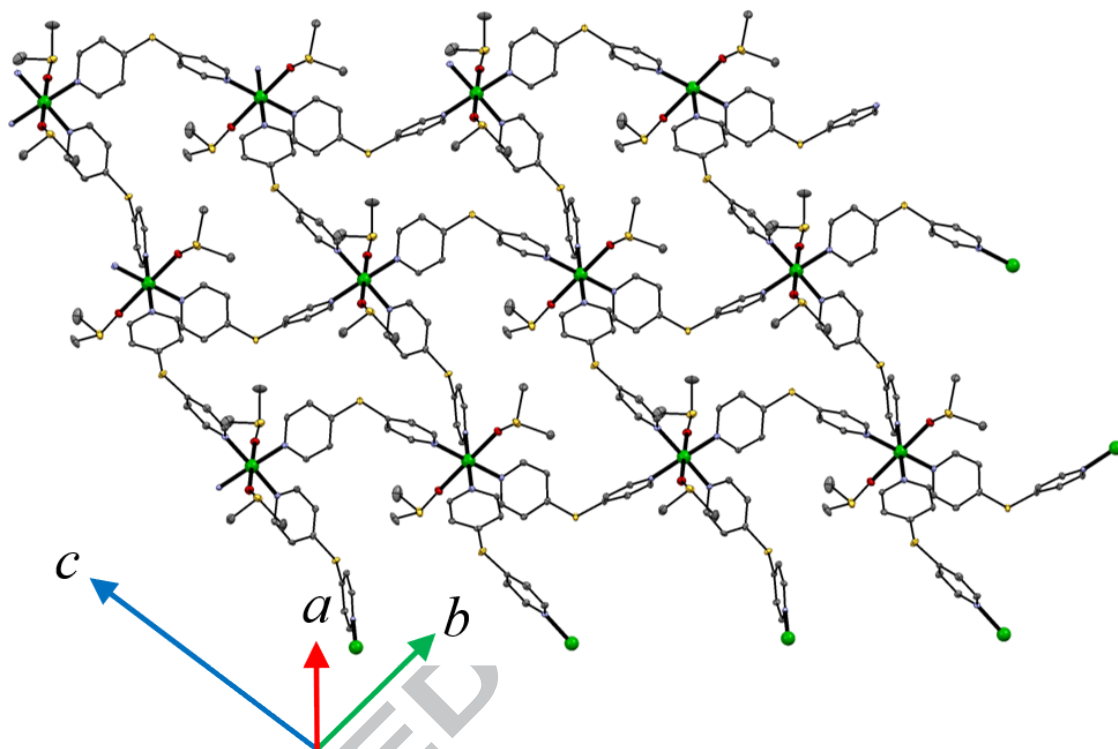


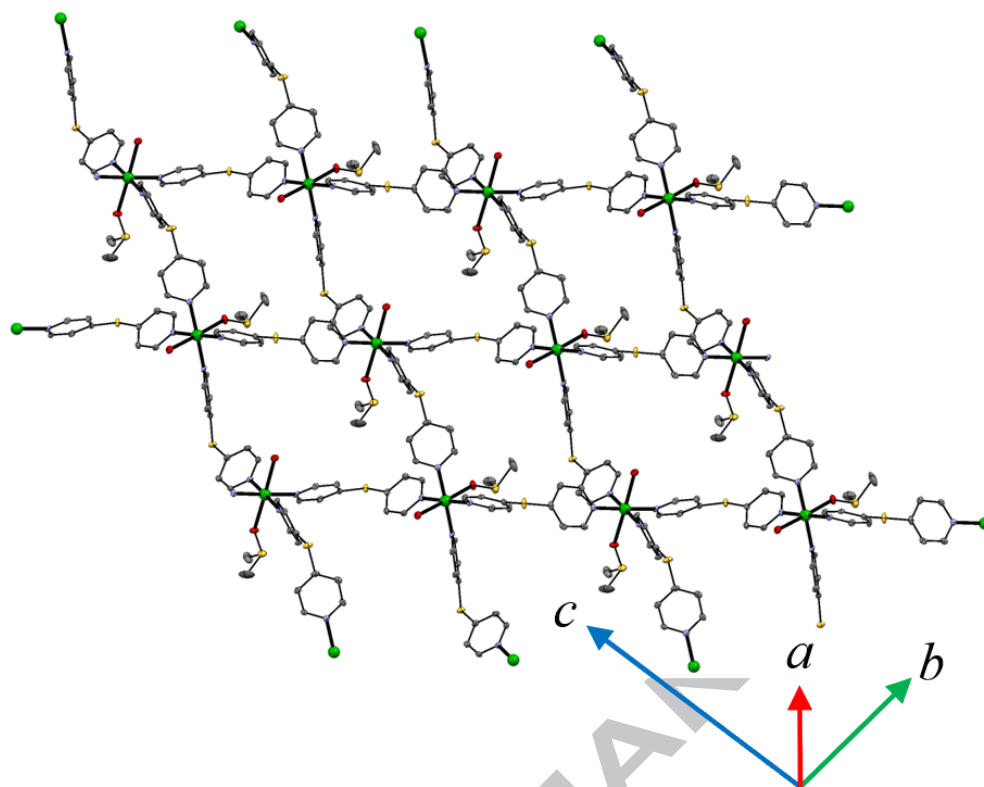
Figure 3. View of the crystal structure depicting the metal surroundings ((a) and (c)) and polyhedra ((b) and (d)) of both crystallographic independent copper (II) ions in compound **3** with the numbering of the non-hydrogen and non-carbon atoms. Thermal ellipsoids are drawn at the 50% probability level, and the hydrogen atoms are omitted

for the sake of clarity. Symmetry codes: (i) $x, -y+2, z+1/2$; (ii) $x, -y+1, z+1/2$; (iii) $x, -y+2, z-1/2$; (iv) $x, -y+1, z-1/2$; (v) $x, -y, z+1/2$; (vi) $x, -y, z-1/2$.

(a)



(b)



(c)

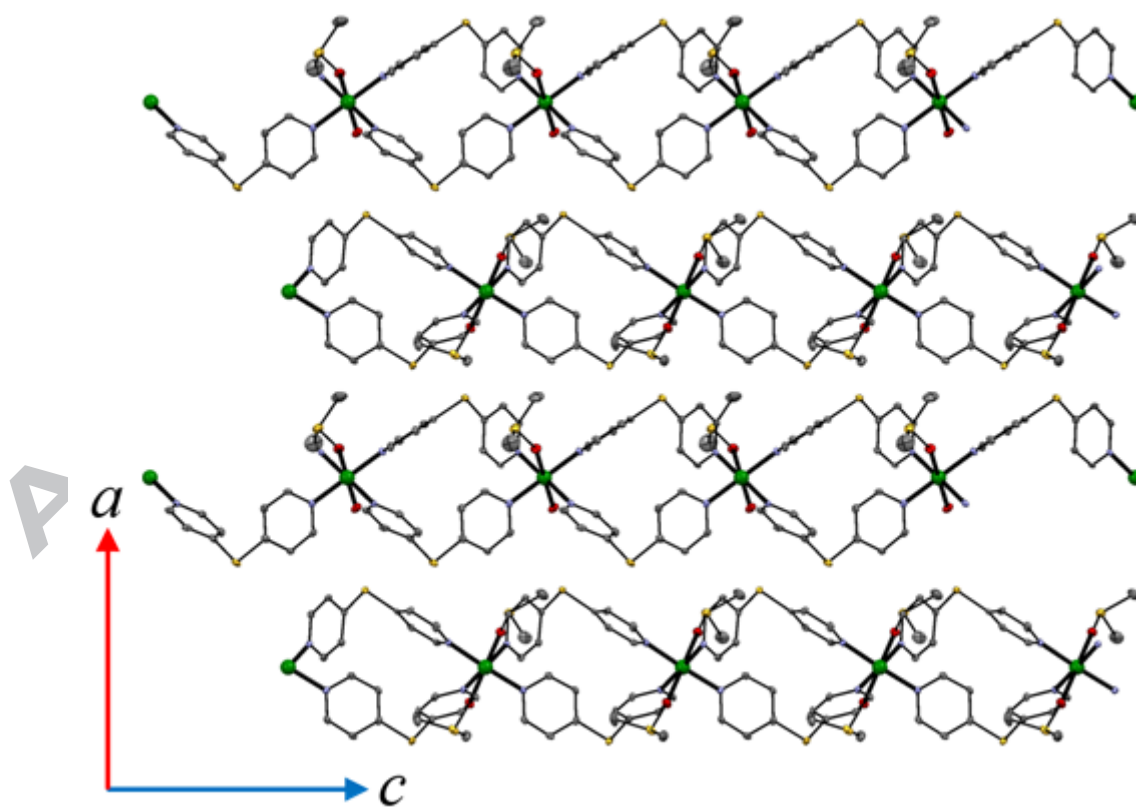


Figure 4. View of a fragment of the cationic layers of **3** concerning the extension of Cu1 – [Cu(dps)₂(dmsO)(H₂O)]_n²ⁿ⁺ – (a) and Cu(2) – [Cu(dps)₂(dmsO)₂]_n²ⁿ⁺ – (b) crystallographic independent units. Crystallization solvent molecules and perchlorate anions were omitted for the sake of clarity. (c) View of the ABAB arrangement of the cationic layers – Cu1-Cu2-Cu1-Cu2 layers– in **3** extending in the crystallographic plane *ac*.

3.3. Magnetic Properties

The magnetic susceptibility of crushed polycrystalline samples of **1-3** was investigated in the temperature range 2-300 K under an applied dc magnetic field of 1 kOe. The magnetic behaviors of the complexes are shown in Figure 5 in the form of $\chi_M T$ versus T plot, with χ_M being the magnetic susceptibility per cobalt unit (**1**) or per copper(II) units (**2** and **3**).

At room temperature, the $\chi_M T$ product for **1** is 2.47 cm³ mol⁻¹ K and remains constant upon cooling until approximately 180 K. At lower temperatures, $\chi_M T$ further decreases continuously to 1.55 cm³ mol⁻¹ K at 2.0 K. The $\chi_M T$ value at room temperature is greater than expected for a magnetically isolated spin quartet (1.875 cm³ mol⁻¹ K for $S_{Co} = 3/2$) with $g = 2.00$, indicating that a significant orbital contribution may be involved [50-51]. Indeed, if we analyse this system through a simple Curie-Weiss law expression [51], with a θ parameter accounting for the very weak magnetic intermolecular interactions between the metal ions, the theoretical curve (solid line in Figure S5) did not match well the experimental data ($g = 2.28$, $\theta = -4.8$ K, and the agreement factor R , defined as $\sum[(\chi_M T)_{obs} - (\chi_M T)_{calc}]^2 / \sum[(\chi_M T)_{obs}]^2$, of $4.2 \cdot 10^{-3}$). This behavior is compatible to a system with $S \geq 1$ spin ground state, which can be subjected to a zero-field splitting (ZFS) that arises through the coupling of the ground state with

excited states via spin-orbit coupling. Thus, the following expressions for the magnetic susceptibility for $S = 3/2$ are applicable (Equations 1 and 2) [51]:

$$\chi_{\parallel} = \frac{Ng^2\beta^2(1 + 9\exp(-2D/kT))}{4kT(1 + \exp(-2D/kT))} \quad (1)$$

$$\chi_{\perp} = \frac{Ng^2\beta^2(1 + (3kT/4D)[1 - \exp(-2D/kT)])}{kT(1 + \exp(-2D/kT))} \quad (2)$$

Where g is the average Landé factor of the cobalt(II) ions, D is the magnitude of the ZFS, N , β , and k have their usual meanings. The average molar magnetic susceptibility for a powder sample is given by Equation 3.

$$\chi_M = \frac{\chi_{\parallel} + 2\chi_{\perp}}{3} \quad (3)$$

For this model, least-squares best-fit parameters are $D = 54.0 \text{ cm}^{-1}$, $g = 2.31$, and the agreement factor $R = 2.6 \times 10^{-5}$. The theoretical curve (solid line in the corresponding curve in Figure 5) match well the experimental data. Thus, the main contribution to the decrease of the $\chi_M T$ values at lower temperatures may be attributed to ZFS effects.

Alternating current (ac) magnetic susceptibility data were measured for **1** in order to investigate the occurrence of slow relaxation of the magnetization. Under a zero static dc field, no significant frequency dependency was observed for both in-phase (χ') and out-of-phase (χ'') susceptibility components. This behavior suggests a quantum tunneling of the magnetization (QTM) which may arise from dipolar and/or hyperfine interactions. When the ac measurements were performed in the presence of a static dc field (H_{DC}) of 1.0 kOe the QTM was partly or wholly suppressed and then χ' and χ'' showed typical single-ion magnets behavior, see Fig. 6 (a) and (b). Quantitative determination of the relaxation time (τ) was obtained by fitting $\chi'(v)$ and $\chi''(v)$ curves obtained at different temperatures with the generalized Debye equation [52] (Fig. 6 (a) and (b) and Table S4, SI). The achieved parameters of the Debye model and the $\chi'(v)$ and

$\chi''(\nu)$ data were used in constructing the Argand (Cole-Cole) diagram, as shown in Fig. 7 (a). The Cole-Cole plots exhibit semicircular shapes with α values within the range 0.01-0.14, indicating a narrow distribution of the relaxation processes ($\alpha = 0$ for a single relaxation process). To gain further insights into the mechanisms of the slow relaxation of the magnetization, we study the temperature dependence of τ , see Fig. 7 (b). The fit of the linear portion of the data using the exponential Arrhenius expression afforded an effective energy barrier for the reversal of magnetization of 22.9 (1.1) K and $\tau_0 = 5.3 (1.2) \times 10^{-7}$ s. The deviation of the data from the Arrhenius law at low temperatures indicates the existence of other relaxation process for **1**. Since for an applied field of 1.0 kOe the QTM is expected to be insignificantly, we fitted the temperature dependence of the relaxation time using the following model [53]:

$$\tau^{-1} = AT + CT^n \quad (4)$$

Where the first term represents the rate of the direct process, and the second is the rate of the Raman process. Best-fits results gave the following set of parameters (values in parentheses are the standard errors): $A = 414 \text{ s}^{-1} \text{ K}$, $C = 9.3(1.6) \text{ s}^{-1} \text{ K}^{-n}$ and $n = 4.7(2)$. The obtained n value is found similar to the reported values for Co^{2+} ions [54-55]. Consequently, the deviation from linearity observed in Fig.7(b) might be explained by considering the direct process which is dominant at low temperature and the Raman process which is responsible for the increase of the relaxation time at high temperature. No reasonable fit could be obtained by considering only a Raman process.

Taking into consideration compounds **2** and **3**, the $\chi_M T$ product at room temperature are 0.46 and 0.45 $\text{cm}^3 \text{ K mol}^{-1} \text{ K}$, respectively, which are in agreement with the expected value for a magnetically isolated spin doublet ($S_{\text{Cu}} = 1/2$) with $g = 2.20$. Upon cooling, $\chi_M T$ product remains constant until approximately 20 K and further decrease slightly to attain values of 0.45 (**2**) and 0.43 $\text{cm}^3 \text{ mol}^{-1} \text{ K}$ (**3**) at 2.0 K. This

behavior is typical of a very weak antiferromagnetic interaction between the copper(II) ions in the two-dimensional network, which could be regarded as a sheet-like architecture based on a rhombus-shaped Cu₄ cyclic motif as building unit. The same Cu₄ motif is observed for compound **2** and in both layers of compound **3**. The Cu₄ motif presents Cu–Cu distances of 10.1553(8) and 10.3402(8) Å (**2**), 10.4516(9) and 10.4868(9) Å ([Cu(dps)₂(dmsO)₂]_n²ⁿ⁺ fragment of **3**), and 10.4387(9) and 10.4998(9) Å ([Cu(dps)₂(dmsO)(H₂O)]_n²ⁿ⁺ fragment of **3**), as shown in Figure 8 (for **2** only as illustrative purposes, although the same analysis can be extended for the two layers of compound **3** since their Cu₄ units are very similar). Considering this Cu₄ motif, the magnetic data were analysed through the theoretical expression for an extended copper(II) antiferromagnetic quadratic-layer network with local spins $S = 1/2$, for both **2** and **3** (Equation 5)[56].

$$\chi_M = \frac{N\beta^2 g^2}{J} \left\{ 3\Theta + \sum_{n=1}^6 \frac{C_n}{\Theta^{n-1}} \right\}^{-1} \quad (5)$$

The Hamiltonian being $\hat{H} = -J \sum_{i,j} \hat{S}_i \cdot \hat{S}_j$, i and j represent the nearest neighbours spins, $\Theta = kT/J S(S+1)$, J is the intramolecular exchange interaction between Cu²⁺ ions in the Cu₄ motif, S_i and S_j are the spin operators for each $S = 1/2$ Cu²⁺ center, $C_1 = 4$, $C_2 = 2.667$, $C_3 = 1.185$, $C_4 = 0.149$, $C_5 = -0.191$, $C_6 = 0.001$, g is the average Landé factor of the copper(II) ions and N , β and k have their usual meanings. Least-squares best-fit parameters through Equation 4 are $J = -0.05$ cm⁻¹, $g = 2.22$ and $R = 2.4 \times 10^{-6}$ for **2** and $J = -0.10$ cm⁻¹, $g = 2.21$ and $R = 3.3 \times 10^{-5}$ for **3**.

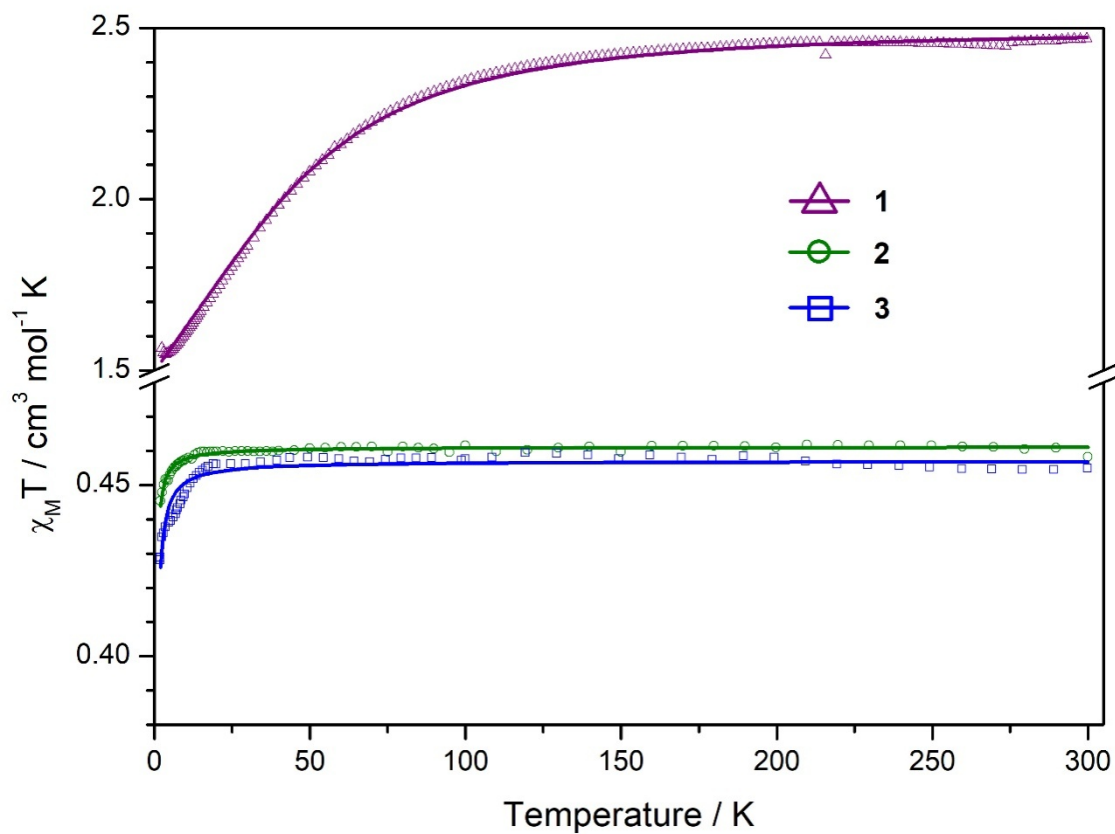


Figure 5. $\chi_M T$ vs. T plot for **1** (purple triangles), **2** (green circles) and **3** (blue squares). Best-fit curves through Equations 1-3, for **1**, or Equation 4, for **2** and **3** (see text) are shown as solid lines.

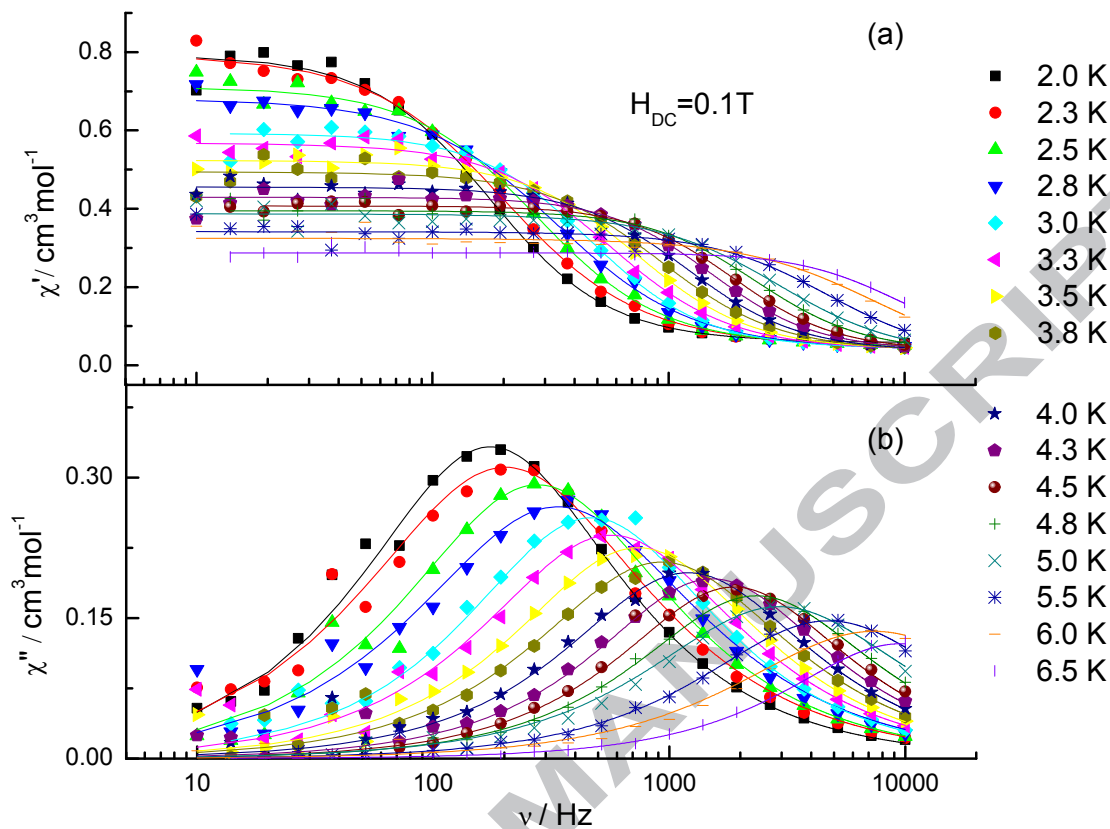


Figure 6. Frequency dependency of the in-phase (a) and out-of-phase (b) components of ac magnetic susceptibility plots for **1** under static applied field of 1kOe in the frequency range of 10-10000 Hz. The solid lines represent the best-fit curves based on the generalized Debye equation.

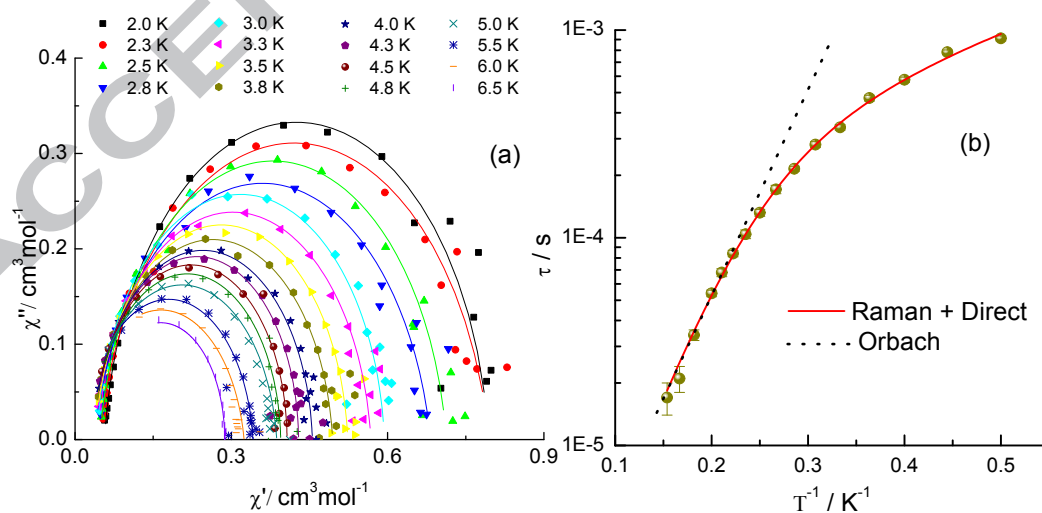


Figure 7. (a) Cole-Cole plots for **1** under an applied field of 1.0 kOe in the frequency range of 10-10000 Hz. The solid lines represent the best fits based on the generalized Debye equation. (b) Temperature dependency of the average relaxation time for **1** at 1.0 kOe dc applied field. The experimental data have been fitted with Orbach, Raman, and Direct processes.

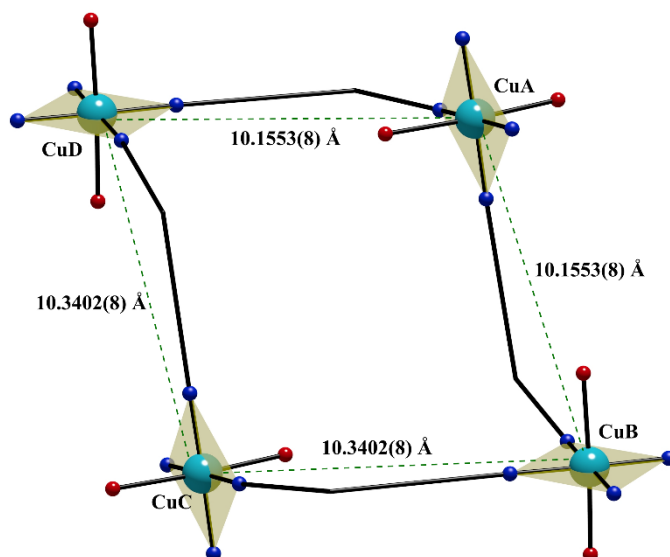


Figure 8. View of the rhombus-shaped Cu_4 cyclic motif of the antiferromagnetic quadratic layer for **2**, with copper(II) ions as light blue spheres, oxygen and nitrogen atoms as red and dark blue spheres, respectively. The light yellow planes represent the basal plane associated with the magnetic $d_{x^2-y^2}$ orbitals (see text).

Previous studies of dps based coordination compounds have shown that dps bridges are very poor mediators of magnetic interactions, for example as extended double bridges between copper(II) ions [16,19]. For compounds **2** and **3**, the metal ions are linked by the dps ligand in a bis-monodentate bridging mode through an out-of-plane exchange pathway as shown in Figure 8 (CuA–CuB and CuC–CuB), which contributes to a poor overlap of the magnetic orbitals. In addition, due to dps flexibility, the adjacent copper magnetic orbitals, which lies on the basal plane formed by the $\text{Cu-N}_{4(\text{dps})}$ atoms due to the distorted Jahn-Teller octahedron coordination sphere of each

copper(II) ion [being $d_{x^2-y^2}$ type magnetic orbital], are oriented in a quasi-orthogonal mode (angles between basal planes of 86.05° for **2** and 85.85° for the $[\text{Cu}(\text{dps})_2(\text{dmsO})_2]_n^{2n+}$ fragment of **3**) or strongly deviates from planarity (77.36° for the $[\text{Cu}(\text{dps})_2(\text{dmsO})(\text{H}_2\text{O})]_n^{2n+}$ fragment of **3**). Since both the long copper–copper distances as well as the lack of proper orientation of magnetic orbitals along the exchange pathway contribute to the poor magnetic interaction between metal ions in compounds **2** and **3**, the magnetic data could be analysed through a simple Curie-Weiss law expression with a θ parameter accounting for the very weak paramagnetic centres interactions. For this model, least-squares best-fit parameters are: $\theta = -0.08$ K, $g = 2.22$ and $R = 2.4 \times 10^{-6}$ for **2** and $\theta = -0.14$ K, $g = 2.21$ and $R = 3.2 \times 10^{-5}$ for **3**. The theoretical curves (Figure 5 and Figure S5 of Supplementary Information) match well the experimental data in both antiferromagnetic quadratic-layer or Curie models, with similar agreement factors. The very small J and θ values reflect the very poor mediation of magnetic interactions induced by the extended bis-monodentatedps bridges.

4. Conclusions

This work reports the synthesis and crystal structures of three compounds containing cobalt (**1**) and copper (**2-3**) with the dps ligand. The X-ray diffraction data revealed that **1** is a mononuclear cobalt(II) compound in which the metal ion is six-coordinated, and its coordination sphere is composed by four dps ligands and two water coordination molecules in *trans*-positions. The crystallographic data for **2** and **3** revealed that these are two-dimensional coordination polymers, where the copper ions are coordinated to four dps ligands in the equatorial plane and two distal solvent molecules in the apical positions resulting in a 2D (4,4)-net, which is made of rhombus shaped Cu_4 cyclic motifs with four-connected copper nodes and bis(monodentate) dps ligands. It is worth

noting that the crystal structure of **3** is similar to **2**; however, one copper(II) in the bidimensional structure is coordinated by two dmsu molecules whereas the other metal ion has one dimethylsulfoxide and one water molecule in its coordination sphere, so the unit cell passes from orthorhombic to triclinic when comparing **2** and **3**. In this work, the dimensionality of the systems was driven by the nature of the metal ion. The cobalt ions led to the formation of the mononuclear system, even with a large excess of metal ions in the synthesis, while the copper ions led to the formation of two-dimensional systems, even using different solvents and crystallization methods. Magnetic properties of **1-3** were investigated in the polycrystalline samples of these compounds. The results show that **1** is a mononuclear cobalt(II) compound that exhibit a field-induced slow relaxation of the magnetization behaving as single-ion magnet while **2** and **3** present, in practice, a magnetic behavior of mononuclear copper(II) complexes as a result of the largest separations between metal ions in each rhombus-shaped Cu₄ cyclic motif of *ca.* 10 Å. In fact, the antiferromagnetic coupling constants (J) between copper(II) ions in **2** and **3** are very small ($J = -0.05 \text{ cm}^{-1}$ (**2**) and $J = -0.10 \text{ cm}^{-1}$ (**3**)), typical of a very weak antiferromagnetic interaction among the metal ions in the two-dimensional network.

ACKNOWLEDGMENTS

This work was supported by Conselho Nacional de Desenvolvimento Científico e Tecnológico (CNPq, Grants 405199/2016-3; 309687/2018-7), Fundação de Amparo à Pesquisa do Estado de Minas Gerais (FAPEMIG, Grant PPM00508-16), Fundação de Amparo à Pesquisa do Estado de São Paulo (FAPESP, Grant 2015/22379-7) Coordenação de Aperfeiçoamento de Pessoal de Nível Superior (CAPES-Finance code 001).

REFERENCES

- [1] N. R. Campos, M. A. Ribeiro, W. X. C. Oliveira, D. O. Reis, H. O. Stumpf, A. C. Doriguetto, F. C. Machado, C. B. Pinheiro, F. Lloret, M. Julve, J. Cano, M. V. Marinho, *Dalton Trans.*, 2016, **45**, 172.
- [2] N. D. la Pinta, A. B. Caballero, G. Madariaga, J. M. Ezpeleta, A. Rodriguez-Diequez, J. M. Salas, R. Cortés, *CrystEngComm*, 2014, **16**, 8322.
- [3] B. Manna, S. Singh, A. Karmakar, A.V. Desai, S. K. Ghosh, *Inorg. Chem.* 2015, **54**, 110-116.
- [4] M. Sánchez-Serratos, J. R. Álvarez, E. González-Zamora, I. A. Ibarra, *J. Mex. Chem. Soc.* 2016, **60**(2), 43.
- [5] H. Furukawa, K. E. Cordova, M. O’Keeffe, O. M. Yaghi, *Science*, 2013, **341**, 1230444.
- [6] J. Parreiras, E. N. Faria, W.X.C. Oliveira, W.D. do Pim, R.V. Mambrini, E.F. Pedroso, M. Julve, C.L.M. Pereira, H.O. Stumpf, *J. Coord. Chem.* 2018,**71**, 797-812.
- [7] B.-C. Tzeng, H.-T. Yeh, T.-Y. Chang, G.-H. Lee, *Cryst. Growth Des.*, 2009, **9**, 2552.
- [8] T. R. G. Simões, R. V. Mambrini, D. O. Reis, M. V. Marinho, M. A. Ribeiro, C. B. Pinheiro, J. Ferrando-Soria, M. Déniz, C. Ruiz-Pérez, D. Cangussu, H. O. Stumpf, F. Lloret, M. Julve, *Dalton Trans.*, 2013, **42**, 5778.
- [9] M. V. Marinho, M. I. Yoshida, K. J. Guedes, K. Krambrock, A. J. Bortoluzzi, M. Hörner, F. C. Machado, W. M. Teles, *Inorg. Chem.*, 2004, **43**, 1539.
- [10] T. R. G. Simoes, W. D. do Pim, I. F. Silva, W. X. C. Oliveira, C. B. Pinheiro, C. L. M. Pereira, F. Lloret, M. Julve, H. O. Stumpf, *CrystEngComm*, 2013, **15**, 10165.

- [11] W. D. do Pim, T. R. G. Simões, W. X. C. Oliveira, I. R. A. Fernandes, C. B. Pinheiro, F. Lloret, M. Julve, H. O. Stumpf, C. L. M. Pereira, *Cryst. Growth Des.* 2014, **14**, 5929.
- [12] L. F. Marques, M. V. Marinho, C. C. Corrêa, N. L. Speziali, R. Diniz, F. C. Machado, *Inorg. Chim. Acta*, 2011, **368**, 242.
- [13] M. V. Marinho, L. F. Marques, D. S. Maia, N. L. Speziali, M. I. Yoshida, J. Janczak, M. Horner, C. C. Corrêa, R. Diniz, F. C. Machado, *Z. Anorg. Allg. Chem.* 2015, **641**, 2333.
- [14] M. V. Marinho, L. C. Visentin, M. C. De Souza, R. Diniz, K. Krambrock, M. I. Yoshida, F. C. Machado, *Polyhedron*, 2010, **29**, 2657.
- [15] M. V. Marinho, M. I. Yoshida, K. Krambrock, L. F. C. De Oliveira, R. Diniz, F. C. Machado, *J. Mol. Struct.*, 2009, **923**, 60.
- [16] M. V. Marinho, L. F. Marques, R. Diniz, H. O. Stumpf, L. C. Visentin, M. I. Yoshida, F. C. Machado, F. Lloret, M. Julve, *Polyhedron*, 2012, **45**, 1.
- [17] G. A. M. Sáfar A. Malachias, R. Magalhães-Paniago, M. V. Marinho, H. O. Stumpf, *J. Phys. Chem. C.*, 2012, **116**, 25611.
- [18] L. Croitor, E. B. Coropceanu, D. Chisca, S. G. Baca, J. van Leusen, P. Kögerler, P. Bourosh, V. Ch. Kravtsov, D. Grabco, C. Pyrtsac, M. S. Fonari, *Cryst. Growth Des.*, 2014, **14**, 3015.
- [19] L. Tang, L. Gao, F. Fu, J. Cao, D. Chao, *Z. Anorg. Allg. Chem.* 2014, **640**, 1368.
- [20] S. Muthu, Z. Ni, J. J. Vittal, *Inorg. Chim. Acta*, 2005, **358**, 595.
- [21] Q.-F. Xu, Q.-X. Zhou, J.-M. Lu, X.-W. Xia, L.-H. Wang, Y. Zhang, *Polyhedron*, 2007, **26**, 4849.

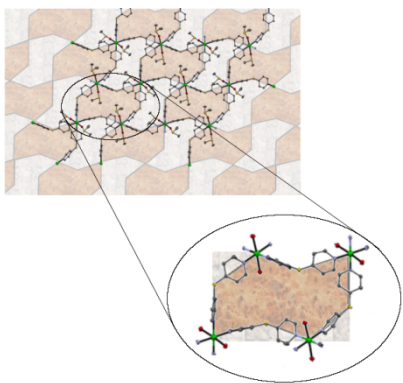
- [22] X. Feng, R.-L. Zhang, X.-G. Shi, F. Ruan, *Z. Kristallogr.* 2009, **224**, 258.
- [23] L. Croitor, E. B. Coropceanu, D. Chisca, S. G. Baca, J. van Leusen, P. Kögerler, P. Bourosh, V. Ch. Kravtsov, D. Grabco, C. Pyrtsac, M. S. Fonari, *Cryst. Growth Des.*, 2014, **14**, 3015.
- [24] J.-F. Lu, Q.-F. Xu, Q.-X. Zhou, Z.-L. Wang, J.-M. Lu, X.-W. Xia, L.-H. Wang, Y. Zhang, *Inorg. Chim. Acta*, 2009, **362**, 3401.
- [25] J.-X. Li, Z.-X. Du, J. Zhou, H.-Q. An, S.-R. Wang, B.-L. Zhu, S.-M. Zhang, S.-H. Wua, W.-P. Huang, *Inorg. Chim. Acta*, 2009, **362**, 4884.
- [26] X.-J. Sun, L.-Y. Xu, J.-F. Ge, Q.-F. Xu, J.-M. Lu, *Polyhedron*, 2011, **30**, 997.
- [27] J. Zhao, D.-S. Li, Y.-P. Wu, J.-J. Yang, W.-W. Dong, K. Zou, *Inorg. Chem. Commun.*, 2013, **35**, 61.
- [28] Y. Niua, Z. Li, Y. Song, M. Tanga, B. Wua, X. Xin, *J. Solid State Chem.* 2006, **179**, 4003.
- [29] Lin, R.-B., Li, L., Wu, H., Arman, H., Li, B., Lin, R.-G., Zhou, W., Chen, B. *J. Am. Chem. Soc.* 2017, **139**, 8022.
- [30] L.-F. Ma, Y.-Y. Wang, L.-Y. Wang, D.-H. Lu, S. R. Batten, J.-G. Wang, *Cryst. Growth Des.*, 2009, **9**, 2036.
- [31] D. Yang, H. Zhou, A.-H. Yuan, Y.-Z. Lid, *CrystEngComm*, 2014, **16**, 8344.
- [32] G. A. Bain, J. F. Berry, *J. Chem. Educ.*, 2008, **85**, 532.
- [33] A. Earnshaw, *Introduction to Magnetochemistry*, Academic Press, London, 1968.
- [34] CrysAlisPro, Rigaku Oxford Diffraction, CrysAlisPro Software system, Rigaku Corporation, Oxford, UK, 2015.

- [35] *APEX3*. Bruker AXS Inc., Madison, Wisconsin, USA, 2012.
- [36]. Sheldrick, G. M. (2001). XPREP. Bruker-AXS, Madison, Wisconsin, USA.
- [37] L. Palatinus, G. Chapuis, *J. Appl. Cryst.* 2007, **40**, 786.
- [38] L. Palatinus, S. J. Prathapa, S. van Smaleen. *J. Appl. Cryst.* 2012, **45**, 575.
- [39] G. M. Sheldrick, SHELX – Programs for crystal structure determination (SHELXS) and refinement (SHELXL), *Acta Cryst.* (2008) **A64**, 112,
- [40] G. M. Sheldrick, SHELX – Programs for crystal structure determination (SHELXT), *Acta Cryst.* 2015, **A71**, 3.
- [41] G. M. Sheldrick, SHELX – Programs for crystal structure refinement (SHELXL-2014), *Acta Cryst.* 2015, **C71**, 3.
- [42] C. K. Johnson, ORTEP, Crystallographic Computing, edited by F. R. Ahmed, pp 217-219, Copenhagen, Denmark.
- [43] R.C. Clark, J.S. Reid, *Acta Cryst.* 1995, **A51**, 887.
- [44] S. Parsons, H. D. Flack, T. Wagner, *Acta Cryst.*, 2013, **B65**, 249.
- [45] C. K. Johnson, in Crystallographic Computing, ed. F. R. Ahmed, Copenhagen, Denmark, 1970, pp. 217.
- [46] F. Macrae, P. R. Edgington, P. McCabe, E. Pidcock, G. P. Shields, R. Taylor, M. Towler and J. Streek van der, *J. Appl. Crystallogr.*, 2006, **39**, 453.
- [47] C. Chailuecha, S. Youngme, C. Pakawatchai, N. Chaichit, G. A. van Albada, J. Reedijk, *Inorg. Chim. Acta*, 2006, **359**, 4168-4178.
- [48] K. Nakamoto, *Infrared and Raman Spectra of Inorganic and Coordination Compounds*, fourth ed., Wiley Interscience, New York, 1986.

- [49] W. X. C. Oliveira, M. A. Ribeiro, C. B. Pinheiro, M. M. da Costa, A. P. S. Fontes, W. C. Nunes, D. Cangussu, M. Julve, H. O. Stumpf, C. L. M. Pereira, *Cryst. Growth Des.* 2015, **15**, 1325-1335.
- [50] F. Lloret, M. Julve, J. Cano, R. Ruiz-García, E. Pardo, *Inorg. Chim. Acta*, 2008, **361** 3432–3445.
- [51] O. Kahn, *Molecular Magnetism*, Wiley-VCH, Weinheim, 1993.
- [52] K. S. Cole, R. H. Cole, *J. Chem. Phys.*, 1941, **9**, 341-351
- [53] A. Abragam, B. Bleaney, *Electron Paramagnetic Resonance of Transition ions*, Reprint 20, Oxford University Press, Oxford, 1970.
- [54] E. Colacio, J. Ruiz, E. Ruiz, E. Cremades, J. Krzystek, S. Carretta, J. Cano, T. Guidi, W. Wernsdorfer, E. K. Brechin, *Angew. Chem Int. Ed*, 2013, **52**, 9130-9134.
- [55] A. K. Mondal, A. Mondal, B. Dey, S. Konar, *Inorg Chem.*, 2018, **57**, 9999-10008
- [56] M. E. Lines, *J. Phys. Chem. Solids*, 1970, **31**, 101-116.

Synopsis

Synthesis, crystal structures and magnetic properties of one mononuclear cobalt(II) complex and two-bidimensional corrugated brick-wall architectures containing copper(II) ions driven by a flexible ligand were developed.



ACCEPTED MANUSCRIPT